

**Core planar cell polarity function in migrating gastrula cells – analysis of a novel zebrafish
prickle1a mutant line**

McKenna Edwards

**A Thesis Submitted in Partial Fulfillment of the Requirements for Degree of Master
of Science**

Middle Tennessee State University

March 2023

Thesis Committee:

Jason Jessen, PhD., Chair

April Weissmiller, PhD.

Brian Robertson, PhD.

ACKNOWLEDGEMENTS

This research project would not have been possible without the expertise and guidance of my mentor and thesis advisor, Dr. Jason Jessen. I want to give a huge thank you for all the help and support he has provided me throughout my time in his lab and working on this project. Without his aid both in the lab and the writing process, I would not have been able to come this far. I am also immensely grateful for Dr. April Weissmiller and Dr. Brian Robertson for being members of my committee and providing helpful advice and feedback throughout this project. Furthermore, I would like to thank my fellow lab mate, Joy Creighton, for her assistance in the laboratory and fish maintenance, as well as her wisdom in performing and troubleshooting lab experiments. I would also like to thank the Graduate Scholarship Committee for awarding me the Mary C. Dunn Summer stipend, which provided financial support for living expenses during my Summer 2022 research. Finally, I would like to thank my God, my parents, and my husband for their tremendous support and encouragement throughout my graduate studies, as well as the financial and mental stability that allowed me to be a part of this program.

ABSTRACT

Planar cell polarity (PCP) is one of the many important events that occur during zebrafish gastrulation, playing a key role in cell movements that underlie convergence and extension (C&E) of the embryonic body axis. Identifying and understanding the driving forces of this phenomenon will provide further insight into the embryonic development of organisms. Previously, numerous studies performed in the fly have established a six-member core protein PCP pathway, however, many details regarding a core PCP pathway in vertebrates have yet to be elucidated. VANGL planar cell polarity protein 2 (*Vangl2*) is the zebrafish ortholog of the fly core PCP protein Van Gogh/Strabismus (*Vang/Stbm*) and has been established as a crucial component of zebrafish PCP. Nonetheless, it is still unclear whether other homologs of the fly core PCP proteins serve similar roles in higher vertebrate organisms, such as zebrafish. In this study, we evaluated *Prickle1a*, which is a zebrafish homolog to another core fly PCP protein (*Prickle*) that is known to interact with *Vangl2*. Using a previously generated nonsense *prickle1a* mutant (the *sa24579* allele), we performed RT-PCR and microinjection of embryos with *prickle1a* mRNA and *vangl2* antisense morpholino to genetically characterize this mutant. Furthermore, we evaluated the morphology, alignment, and directed migration of mediolateral mesodermal cells at the end of gastrulation (tailbud stage) through differential interference contrast microscopy. We also examined defects in the body axis and C&E visualized in live and fixed whole embryos. While the genetic characterization of this mutation is still not fully understood, we did determine that PCP in the *prickle1a sa24579* mutant is interrupted, suggesting that the *Prickle1a* protein is involved in zebrafish PCP.

TABLE OF CONTENTS

Introduction	1
1. Zebrafish gastrulation	1
2. PCP	4
3. PCP Proteins	5
4. Study Aims and Design	7
Materials and Methods	11
Results	17
Discussion	29
References	33

LIST OF FIGURES

Figure 1: Stages and cell movements during zebrafish gastrulation	3
Figure 2: Lateral view of wild type verses <i>prickle1a</i> (sa24579) mutant zebrafish embryos at tailbud stage.....	6
Figure 3: Schematics of Prickle1a polypeptide and <i>prickle1a</i> genomic locus	8
Figure 4: Chromatogram data of <i>prickle1a</i> sa24579 zebrafish genomic DNA samples	9
Figure 5: <i>prickle1a</i> sa24579 RT-PCR shows partial decay of <i>prickle1a</i> mRNA	18
Figure 6: <i>prickle1a</i> fails to suppress a C&E phenotype in mutant embryos	19
Figure 7: <i>prickle1a</i> sa24579 results in a variable C&E phenotype represented by shortened anterior/posterior body axis and broader notochord at tailbud	21
Figure 8: <i>prickle1a</i> sa24579 whole mount <i>in situ</i> hybridization assays show further evidence of a C&E phenotype	22
Figure 9: Low dose injection of <i>vangl2</i> antisense morpholino (MO) oligonucleotide into wild type	23
Figure 10: Analysis of <i>vangl2</i> antisense morpholino (MO) oligonucleotide injected <i>prickle1a</i> mutant embryos	24
Figure 11: Analysis of <i>vangl2</i> antisense morpholino (MO) oligonucleotide injected <i>prickle1a</i> mutant embryos at 28-hour post fertilization (hpf).....	25
Figure 12: <i>prickle1a</i> sa24579 mutation results in disruption of cell migration directness at tailbud.....	27
Figure 13: <i>prickle1a</i> sa24579 mutation results in disruption of cell morphology but not orientation	28

LIST OF TABLES

Table 1. PCR primers	16
Table 2. PCR parameters	16

INTRODUCTION

1. Zebrafish Gastrulation

Vertebrate embryonic development encompasses a series of stages important for multicellular organism growth, that include extensive cell migration and differentiation. Various models have been used to study these stages to better understand the underlying processes at the cellular and molecular level. Zebrafish (*Danio rerio*) is an important vertebrate model organism used to study the phases of embryonic development *in vivo* due to the external fertilization of their eggs and the translucency of their embryos (Nüsslein-Volhard, 2012). An important stage of development this model is often used to study is gastrulation. Gastrulation is regulated by complex cell migration behaviors that result in major tissue rearrangements and cell fate specification. These processes help shape the body plan and lead to formation of three germ layers: endoderm, mesoderm, and ectoderm (Jessen & Solnica-Krezel, 2005). Learning how these processes are regulated is important if we are to understand how organisms undergo proper growth and development.

Zebrafish gastrulation begins at approximately 50% epiboly as blastodermal cells are moving toward the vegetal pole (Warga & Kimmel, 1990). At this point, cells begin internalizing and begin formation of the three main tissue layers (endoderm, mesoderm, and ectoderm). As the epiblast moves vegetally, the germ ring forms at the margin and the underlying hypoblast cells begin to migrate upwards toward the animal pole (Figure 1.A). This internalization process begins at the future dorsal side of the embryo and eventually happens around the entire circumference at the blastoderm margin (Warga & Kimmel, 1990).

Prior to mid-gastrulation (~80% epiboly), regions of mesendodermal cells make an abrupt change in direction and begin to migrate dorsally to initiate narrowing of the mediolateral body

axis (Sepich et al., 2005). This initial dorsal movement consists of non-planar polarized cells that are rounder in shape and have reduced cell-cell contact, with cell migration showing a meandering and “tumbling” phenotype compared to later stages (Prince & Jessen, 2019; Jessen et al., 2002). As time progresses these cells begin to develop a more ovoid shape, becoming elongated, and starting to pack closer together, moving in a more coordinated and direct fashion (Figure 1.C).

These cellular characteristics play an important role in convergence and extension (C&E) of the body axes, which occurs during late gastrulation and early segmentation stages and shapes gastrula tissues through a narrowing (mediolateral tissues) and elongation (anterior-posterior tissues) of the embryonic body axes (Jessen & Solnica-Krezel, 2005). Cells within the chordamesoderm and paraxial mesoderm undergo elongation and intercalation, contributing greatly to C&E of the embryonic body axes (Rozko et al., 2009; Figure 1.B). Cells in the lateral region closer to the dorsal axis also contribute to C&E movements, being dorsally elongated with more packing and moving at a faster rate towards the dorsal axis (Rozko et al., 2009; Figure 1.B). Failure of cells to elongate and position correctly during late gastrulation results in disrupted C&E characterized by shortening and broadening of the body axes. One possible explanation for this is that rounder, unaligned cells may not be able to “pack” together. This would prevent the directed migration of large members of cells toward the embryonic body axis and inhibit dorsal convergence (Prince & Jessen, 2019). Therefore, a key component of C&E is establishment of tissue or planar cell polarity (PCP).

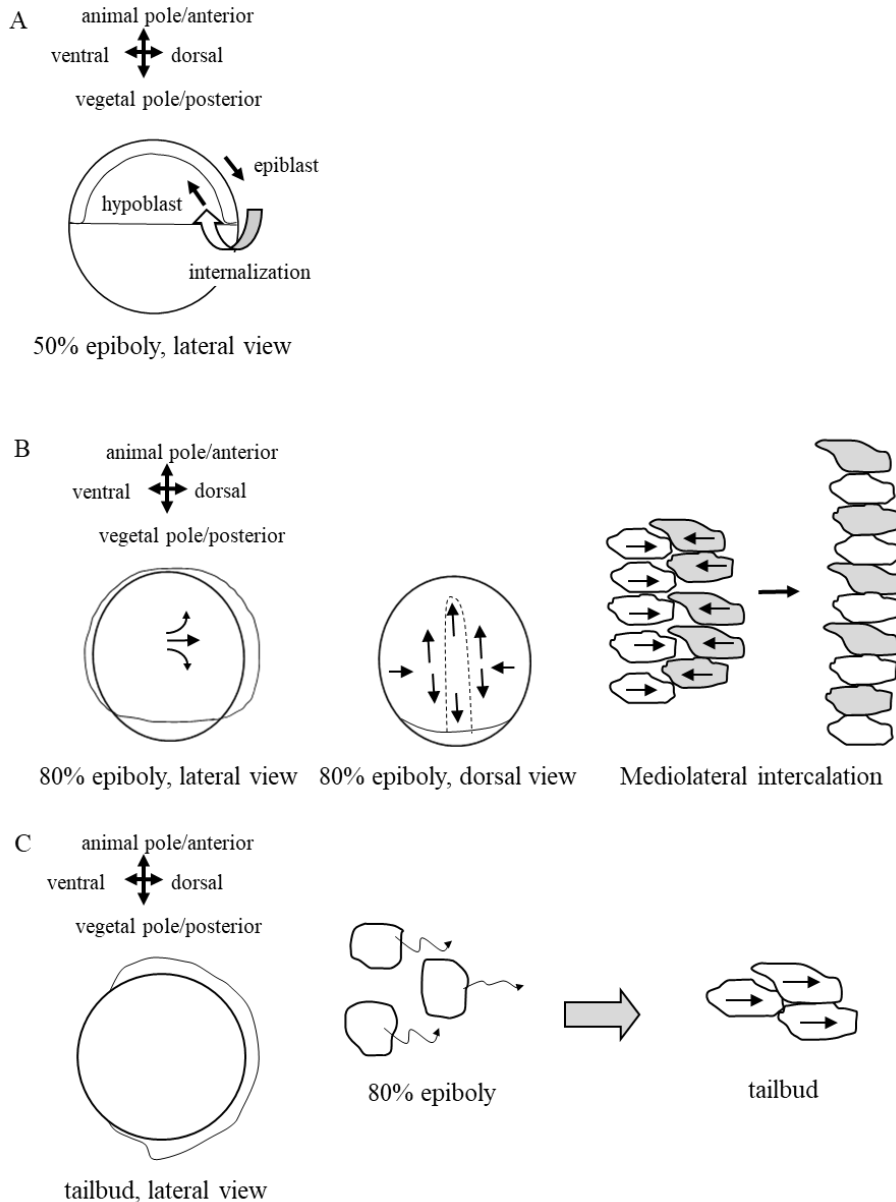


Figure 1. Stages and cell movements during zebrafish gastrulation. (A) The onset of gastrulation begins around 50% epiboly, when cells begin to internalize. The epiblast cells continue to move vegetally while the underlying hypoblast cells move upwards toward the animal pole, beginning the formation of the three germ layers. (B) Close to mid-gastrulation (80% epiboly), lateral mesendodermal cells shift to dorsal migration and begin contributing to convergence and extension (C&E) of the dorsal tissues. Chordamesoderm and paraxial mesoderm cells undergo mediolateral intercalation, further contributing to C&E. Arrows represent direction of cell migration. Rod-like structure seen in the dorsal view represents the notochord. (C) By tailbud (100% epiboly), the yolk is completely enclosed, and lateral mesodermal cells have become more ovoid and elongated in shape. They also pack closer together and increase migration directedness toward the dorsal axis.

2. PCP

First observed in insect cuticles, PCP is defined by the appearance of a coordinated polarity phenotype, evident at the subcellular, cellular, or tissue level, that results from the non-autonomous communication of information between at least two cells (Goodrich & Strutt, 2011). Studies in fruit fly epithelia led to the identification of a six-member core pathway composed of three transmembrane proteins: Van Gogh/Strabismus (Vang/Stbm), Flamingo/Starry Night (Fmi/Stan), and Frizzled (Fz) and three cytosolic proteins: Prickle (Pk), Dishevelled (Dsh), and Diego (Hale and Strutt, 2015).

It has long been established that these proteins are important for the communication of directional information between cells to promote a uniform orientation of subcellular structures (e.g., actin-rich wing hairs) in the fly epithelia. It is believed that the most relevant aspect of fly PCP related to gastrula cells is the polarization of actin-rich structures (Creighton & Jessen, 2020), as changes in actin structure underlie directional cell migration (Caswell & Zech, 2018).

PCP in fly is characterized by two primary features: non-autonomous cell-cell communication and asymmetric protein localization. Loss of protein function in one cell impacts polarity in a neighboring cell, and the effect (e.g. wing hair orientation) depends on the identity of disrupted PCP protein (Taylor et al., 1998; Vinson & Adler, 1987; Goodrich & Strutt, 2011). The function of these proteins is dependent on their asymmetric location both within and between cells. When in their proper location, some of these proteins dimerize, forming both heterodimer and homodimer complexes (Goodrich & Strutt, 2011). Both intercellular and intracellular asymmetry is believed to arise from intracellular feedback signaling mechanisms between adjacent proximal and distal cellular membranes (Tree et al., 2002).

3. PCP Proteins

In fly wing epithelial cells, the three transmembrane proteins (Fmi/Stan, Vang/Stbm, and Fz) are localized to specific regions of the apical cell surface. The proteins form intercellular complexes: Fmi/Stan localizes on both the proximal and distal membrane and forms a homodimer; Vang/Stbm and Fz are asymmetrically located, with Vang/Stbm located proximally and Fz located distally, and the two form a heterophilic complex (Goodrich & Strutt, 2011; Harrison et al., 2020). Loss of core proteins results in planar polarity disruption and a characteristic abnormal wing hair pattern (Wong and Adler, 1993). Additionally, intercellular communication is crucial for epithelial planar polarity in the fly wing, as evident by the ability of mutant cells lacking *vang/stbm* or *fz* to induce abnormal wing hair orientation in neighboring cells (Strutt & Strutt, 2005). Cells lacking Fz induce neighboring cells to point their hairs towards the mutant cell (Vinson & Adler, 1987), and cells lacking Vang/Stbm induce neighboring cells to point their hairs away from the mutant (Taylor et al., 1998).

Despite all that is known about PCP in the fly, many details are lacking regarding the roles of homologous versions of these proteins in vertebrates, including zebrafish. While some of these proteins are involved in PCP independent processes, there is little information about how they specifically regulate vertebrate PCP. A key question is whether a conserved six-member core pathway exists in vertebrates and if these proteins function in the same manner as in fly epithelia (Creighton & Jessen, 2020). The zebrafish Vang/Stbm ortholog VANGL planar cell polarity protein 2 (Vangl2) is essential for polarized cell behaviors during zebrafish gastrulation, regulating mediolateral cell polarity to aid effective C&E cell movements (Jessen et al., 2002). It has been shown that these mutant cells have defects in membrane protrusion number and polarity

(Love et al., 2018; Prince & Jessen, 2019). However, little data has been collected on the roles of other core PCP proteins during zebrafish gastrulation.

One of these lesser studied proteins is Prickle1a, one of five zebrafish Prickle homologs most similar to fly Pk (Creighton & Jessen, 2020). Morpholino-mediated knockdown of zebrafish *prickle1a* translation results in a C&E phenotype (Carreira-Barbosa et al. 2003; Veeman et al. 2003). However, in a recent study, a CRISPR generated *prickle1a* mutant was stated to not have an apparent gastrulation phenotype, with no data shown to support this claim (Ahsan et al., 2019). Preliminary data from the Jessen lab using a novel *prickle1a* nonsense mutant fish line strongly suggested that there is a C&E phenotype present at the end of gastrulation (Figure 2). Therefore, it was important to clearly establish the presence of a C&E phenotype, as well as perform a thorough analysis of cell polarity to determine if the Prickle1a protein is indeed essential for PCP and directed cell migration during zebrafish gastrulation.

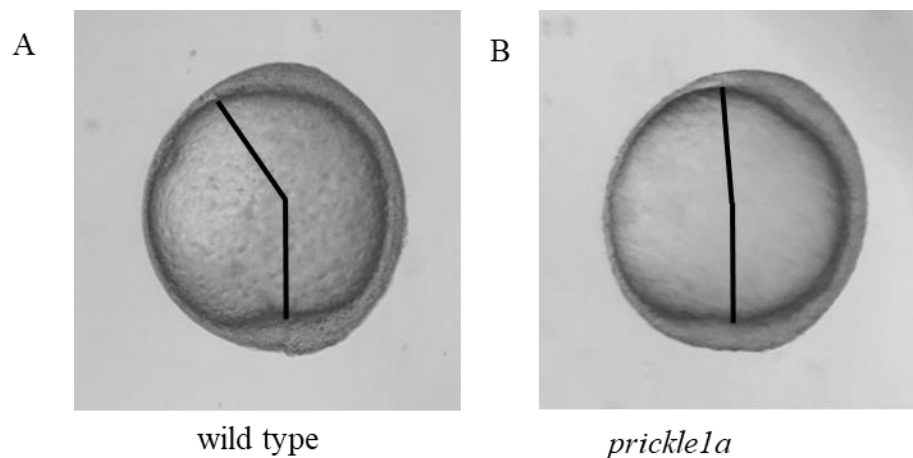


Figure 2. Lateral view of wild type versus *prickle1a* (*sa24579*) mutant zebrafish embryos at tailbud stage. Black lines depict the posterior tail-bud angle. (A) Wild-type live embryo image (B) *prickle1a* mutant live embryo image.

4. Study Aims and Design

In fly, it is known that Pk binding regulates Vang/Stbm protein localization and function (Bastock et al., 2003). It has also been reported that zebrafish Vangl2 and Prickle1a physically bind, and Prickle1a regulates Vangl2 localization to the plasma membrane (Dohn et al. 2013). However, there remains little data supporting the hypothesis that vertebrate Prickle homologs play a conserved role during PCP establishment. Based on previous PCP studies in fly, as well as studies of PCP and Vangl2 in zebrafish, we hypothesized that failure of *prickle1a* to function properly during zebrafish gastrulation would result in a PCP phenotype. The main question of this project was “Do *prickle1a* zebrafish mutants have a PCP phenotype?”, and our goal was to determine and clearly document the severity of this phenotype at the embryo and cellular levels.

To test this hypothesis, *prickle1a* nonsense mutant (*prickle1a* sa24579) fish embryos were examined near the end of gastrulation at 90 – 100% epiboly (yolk plug closure/tailbud), as this is when the *vangl2* mutant phenotype is first detected (Sepich et al., 2000). The *prickle1a* sa24579 mutant was generated by the Derek Stemple lab (Cambridge, United Kingdom). It consists of a cytosine to thymine transition that produces a stop codon at amino acid 596 (Prickle1a has 793 total amino acids) (Kettleborough et al., 2013; Busch-Nentwich et al., 2013; Figure 3.A & B).

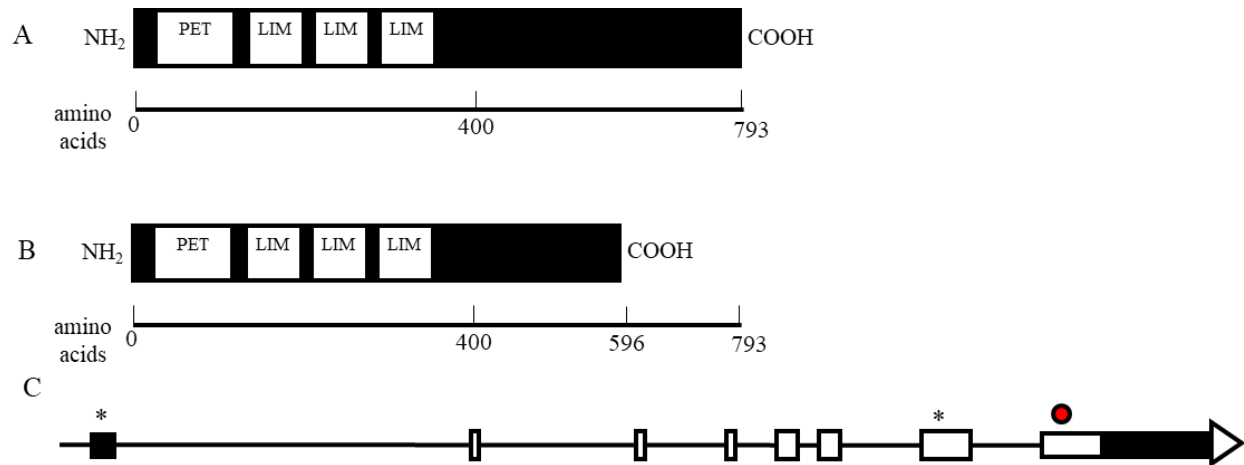


Figure 3. Schematics of *Prickle1a* polypeptide and *prickle1a* genomic locus. (A) Full length *Prickle1a* polypeptide and (B) the hypothetical truncated version due to the *sa24579* stop codon. White boxes with text represent known binding domains. The N and C termini are labeled. (C) Schematic representation of the *prickle1a* transcript. White boxes represent exon translated regions. Black boxes represent exon untranslated regions. *sa24579* stop codon is represented by red dot above the final exon. Black lines indicate introns. Black asterisks represent location of *prickle1a* cDNA primers. White arrow represents direction of translation. Data obtained from (A & B) NCBI Blast and (C) Alliance of Genome Resources.

This premature stop codon is predicted to induce nonsense-mediated mRNA decay. Our chromatogram data obtained from mutant zebrafish genomic DNA samples verified the presence of the C to T mutation in heterozygous adult fin clips (Figure 4.B) and homozygous embryos displaying the C&E phenotype seen in Figure 2.B (Figure 4.C). mRNA levels of tailbud stage embryos were detected using RT-PCR and compared between wild-type embryos and homozygous mutant siblings to determine at what level mRNA decay occurred in the mutant. To verify that the *prickle1a* mutation was the cause of the C&E phenotype, clutches of *prickle1a* *sa24579* embryos were injected with wild-type *prickle1a* mRNA at the single-cell stage and analyzed at tailbud for suppression of the mutant phenotype. Wild-type embryos were also injected with *prickle1a* mRNA to uncover any potential overexpression phenotypes. Alternately, wild type and mutant embryos were injected with low dose (~ 2.5 ng/embryo) *vangl2* antisense morpholino (MO) oligonucleotide (Love et al., 2018). At higher doses in wild type embryos,

vangl2 MO interferes with Vangl2 expression and induces a C&E phenotype (Jessen, 2002). Therefore, worsening of the C&E phenotype in *prickle1a* mutant embryos would indicate a genetic interaction between *prickle1a* and *vangl2*.

To document *prickle1a* mutant phenotypes at the organismal level, live and fixed embryos were analyzed. Brightfield microscopy was used to obtain lateral and dorsal views of live embryos at the tailbud stage. Whole mount *in situ* hybridization assays were used to analyze marker gene expression, an indicator of C&E cell movements, in fixed tailbud stage embryos. These embryos were also imaged using brightfield microscopy.

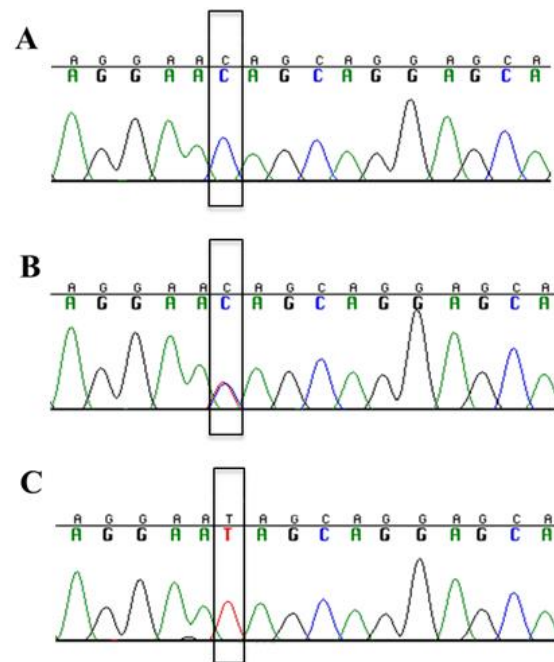


Figure 4. Chromatogram data of *prickle1a* sa24579 zebrafish genomic DNA samples. DNA was obtained from adult fin clips and tailbud stage embryos. *prickle1a* was amplified via PCR, and Sanger sequencing was performed by MC Labs. Black boxes indicate region of interest. (A) *prickle1a* zebrafish fin clip sample showing wild-type sequence. (B) Heterozygous mutant *prickle1a* fin clip sample. (C) Homozygous mutant *prickle1a* tailbud stage embryo sample.

Analyses of cell morphology and migratory behaviors were performed on mutant and wild-type mesodermal cells at the tailbud stage to quantify PCP defects. Polarization of wild-type gastrula stage mesodermal cells is indicated by increased cellular length to width ratios and increased cellular orientation parallel to the path of migration (or perpendicular to the dorsal embryonic body axis). These characteristics are lost in mutants such as *vangl2* that have disrupted PCP signaling (Jessen et al., 2002). Therefore, these cell behaviors were used to analyze and quantify PCP in *prickle1a* sa24579 homozygous mutant embryos as described (Jessen, 2012).

MATERIALS AND METHODS

Zebrafish husbandry and genetic strains

Wild type (AB, TL, and WIK) and homozygous *prickle1a* nonsense mutant (sa24579) (Kettleborough et al., 2013) adult zebrafish (*Danio rerio*) were maintained using standard procedures (Solnica-Krezel et al., 1996). Adult wild type and homozygous *prickle1a* mutant zebrafish mating pairs were crossed with like genetic strains. The embryos resulting from natural spawnings were collected, grown in egg water (60 mg/L Instant Ocean in reverse osmosis water) at either 28.5°C or 32°C, and staged according to morphological criteria (Kimmel et al., 1995).

DNA extraction and sequencing

Adult fin clip samples were obtained and suspended in 250 µL DNA extraction buffer (10 mM Tris pH 8.2, 10 mM EDTA, 200 mM NaCl, 0.5% SDS, 200 mg/mL proteinase K). Samples were incubated at 50°C for 3 hours to overnight. Once the fin-clips were fully dissolved, 500 µL of 100% ethanol was added. Samples were briefly vortexed and stored at -20°C for 30 minutes to overnight and centrifuged 10 minutes at 4°C (15,000 rpm; Eppendorf Centrifuge 5424 R). Supernatant was removed and DNA pellet was washed with 750 µL 70% ethanol and spun at 4°C (15,000 rpm; Eppendorf Centrifuge 5424 R). Supernatant was removed, and the pellet allowed to air dry at room temperature. The DNA pellet was suspended in 100 µL nuclease free water. Polymerase chain reaction (PCR) was performed in a 50 µL reaction volume consisting of 18 µL nuclease free water, 25 µL Promega GoTaq Green Master Mix, 1 µL 10 µM *prickle1a* genotyping forward primer (Table 1), 1 µL 10 µM *prickle1a* genotyping reverse primer (Table 1), and 5 µL DNA template to amplify a 532 base pair DNA fragment containing the mutation site of the *prickle1a* gene. DNA amplification was performed in a Bio-Rad Thermal Cycler (see Table 2 for parameters). PCR products were examined via DNA gel electrophoresis to verify a

single band at 532 base pairs. A 1% (w/v) agarose gel in TAE buffer and Biotium GelRed DNA stain was cast. Biotium Ready-to-Use 1kb DNA ladder (10 μ L) was run alongside 3 μ L PCR product at 100 volts for 30 minutes. The gel was examined via UV light in a Bio-Rad Gel Doc EZ imager and Image Lab Software. Remaining PCR product was then purified via Promega Wizard SV Gel and PCR Cleanup system. Samples were sent to MCLAB for Sanger sequencing.

Reverse transcription polymerase chain reaction (RT-PCR)

Tailbud stage wild type and homozygous *prickle1a* mutant embryos (10 sibling embryos per sample) were manually dechorionated and dissolved in 500 μ L TRIzol. Samples were incubated on ice for 10 minutes. Chloroform (120 μ L) was added, and each tube was vortexed for a minimum of 30 seconds, followed by a 10 minute incubation on ice. Centrifugation was performed at 4 $^{\circ}$ C (15,000 rpm; Eppendorf Centrifuge 5424 R g) for 15 minutes. The upper aqueous layer was placed in a fresh tube and mixed with 0.8 times volume of 100% isopropanol. Samples were incubated on ice for a minimum of 30 minutes and centrifuged at 4 $^{\circ}$ C (15,000 rpm; Eppendorf Centrifuge 5424 R) for 15 minutes. Supernatant was removed, and the pellet was washed with 750 μ L of 70% RNase free ethanol. Centrifugation was performed at 4 $^{\circ}$ C (15,000 rpm; Eppendorf Centrifuge 5424 R) for 5 minutes. Supernatant was discarded, and air-dried RNA pellet was suspended in 20 μ L RNase free water. To check the quality of the total RNA samples, 1 μ L of each was treated with 2 μ L Invitrogen RNA Gel Loading Buffer II at 65 $^{\circ}$ C for 5 minutes. Samples were then run alongside 10 μ L of Biotium Ready-to-Use 1kb DNA ladder on a 1% (w/v) agarose gel in TAE buffer and Biotium GelRed DNA stain. The gel was run at 100 volts for 15 minutes and examined via UV light in a Bio-Rad Gel Doc EZ imager and Image Lab Software. First-strand cDNA was synthesized from 1 μ g of total RNA via the SuperScript III First-Strand Synthesis System for RT-PCR by Invitrogen. PCR was performed in a 50 μ L

reaction volume consisting of 39.25 μL nuclease free water, 5 μL Buffer 3 (Expand Long Template PCR System by Roche), 1.5 μL 10 mM Biosciences deoxynucleotide mix, 0.75 μL 20 μM *prickle1a* cDNA forward primer (Table 1), 0.75 μL 20 μM *prickle1a* cDNA reverse primer (Table 1), 0.75 μL DNA polymerase mix (Expand Long Template PCR System by Roche), and 2 μL cDNA to amplify a 1109 base pair DNA fragment. As a control, primers amplifying a fragment of *cathepsin Lb* (*ctslb*) DNA from the same cDNA samples were also used (Table 1). PCR was performed in a 50 μL reaction volume consisting of 18 μL nuclease free water, 25 μL Promega GoTaq Green Master Mix, 1 μL 10 μM *ctslb* forward primer (Table 1), 1 μL 10 μM *ctslb* reverse primer (Table 1), and 2 μL cDNA template to amplify a 926 base pair DNA fragment. DNA amplification for all samples was performed in a Bio-Rad Thermal Cycler (see Table 2 for parameters). PCR products were examined via DNA gel electrophoresis to compare 1100 bp fragment band intensities between wild type and mutant samples. A 1% (w/v) agarose gel in TAE buffer and Biotium GelRed DNA stain was cast. Biotium Ready-to-Use 1kb DNA ladder (10 μL) was run alongside 6 μL *prickle1a* and 1 μL *ctslb* PCR product at 100 volts for 1 hour. The gel was examined via UV light in a Bio-Rad Gel Doc EZ imager and Image Lab Software.

Embryo microinjection

Microinjection of one-cell stage mutant and wild-type embryos was performed using standard methods (Gilmour et al., 2002). Full-length *prickle1a* DNA (coding sequence) was amplified from cDNA using PCR (see Tables 1 & 2) and cloned into the pCS2+ vector using *dam*⁻/*dcm*⁻ competent *E. coli* cells from New England BioLabs Inc. The pCS2+ vector contains an Sp6 RNA polymerase promoter and a polyadenylation signal sequence, allowing for generation of synthetic mRNAs that will be polyadenylated in the embryo. After ApaI

linearization of the insert/vector clone, synthetic mRNAs were generated using Sp6 RNA polymerase using Invitrogen's mMessage mMachine capped RNA Transcription kit. mRNAs were purified via Roche Quick Spin Columns and mRNAs injected at a concentration of ~ 770 pg/embryo. Embryos were analyzed at tailbud stage for suppression of the *prickle1a* mutant phenotype and induction of an overexpression phenotype in wild type embryos. Alternately, mutant embryos were injected with a low dose (~ 2.5 ng/embryo) of *vangl2* antisense MO oligonucleotide, which induces little to no C&E phenotype in wild type, to determine if it can enhance the *prickle1a* mutant phenotype.

Microscopy

Live mutant and wild-type embryos at tailbud stage were mounted in agarose on coverslip dishes as previously described (Jessen, 2012). Differential interference contrast (DIC) microscopy was performed using an inverted Olympus IX83 microscope with a 40X air-objective (N.A. 0.95) and a Hamamatsu Flash 4.0 CMOS camera to view the lateral mesodermal tissue layer (400X magnification). Low magnification (100X) transmitted light reference pictures were taken to confirm correct orientation of the embryo and notochord position. Time-lapse images of live embryos were collected for 15 minutes at 30 second intervals using Olympus Dimension cellSens software. For whole embryo lateral and dorsal images, live embryos at tailbud were positioned accordingly in 3% methylcellulose. Brightfield images were obtained at 63X magnification on an Olympus SZX16 stereomicroscope with an Olympus Q-Color5 CCD camera and Q-Capture Pro 7 software.

Whole mount in situ hybridization assays

Tailbud stage embryos were fixed overnight in 4% paraformaldehyde in PBS and washed with a PBS/0.1% Tween-20 solution before whole mount *in situ* hybridizations (WISH) were

performed as described (Thisse and Thisse, 2008). Antisense RNA probes for *protocadherin 8* (*pcdh8*), *T-box transcription factor Ta* (*tbxta*), and *distal-less homeobox 3b* (*dlx3*) (markers of the paraxial mesoderm, notochord, and neuroectoderm, respectively) were generated by *in vitro* transcription and purified following standard methods (Westerfield, 2000). Embryos were mounted in a 50/50 solution of WISH staining stop solution (1X PBS pH 5.5, 0.1% Tween20, and 50 mM EDTA) and glycerol on a depression slide and imaged at 63X. Images were obtained using an Olympus SZX16 stereomicroscope with an Olympus Q-Color5 CCD camera and Q-Capture Pro 7 software.

Analysis of PCP and directed migration

Length:width ratios (LWR) and mediolateral alignment (MLA) data were obtained from time-lapse videos generated at 400X magnification using an inverted compound Olympus IX83 microscope as described in section 5. Images were analyzed using Fiji (ImageJ) software, Microsoft Excel, and GraphPad Prism 9. Individual cell trajectory data was obtained from the time-lapse videos using Fiji's Manual Tracking tool. Directness values and cell plot diagrams were generated from the trajectory data using IbiDi's Chemotaxis and Migration Tool (ibidi.com).

Statistics

Data assembly was performed using Microsoft Excel and exported to Prism9 (GraphPad) for graphing and statistical analyses. The type of statistical test performed, and the resulting significance values are noted in the figures and legends, as are the numbers of cells and embryos analyzed for each experiment. The data presented have a normal distribution.

Primer Name	Forward Sequence (5'-3')	Reverse Sequence (5'-3')	Use
<i>prickle1a</i> genotype	GTGCCAAATGAAGTGCCTTA	TTTAGGACGTGACACTCCATGT	Genotyping
<i>prickle1a</i> cDNA	TCTGCTCCTTCACTCCACTG	CTCCCAAACCTGCAGGCTTTG	RT-PCR
<i>prickle1a</i> seq1	CAGCAGCAGGTCAGTGTTG	N/A	Clone verification
<i>prickle1a</i> seq2	CGCAGTGTGAAGATGGGAAA	N/A	Clone verification
<i>prickle1a</i> seq3	CGATGAAGAGCCTGACGTCT	N/A	Clone verification
<i>prickle1a</i> end	CCCAGTACCAGTATTACGCT	N/A	Clone verification
<i>zfprickle1a</i> BamHI	TTACGGATCCGGGGTGTAGTGATG	N/A	Cloning
<i>zfprickle1a</i> XbaI	N/A	TTACTCTAGAAGATTATGACACGTTG	Cloning
<i>ctslb</i>	TGCTCGTCACGCTGTACATA	GCCTTTGTCACCCCATTTGT	RT-PCR

Table 1. PCR primers

Polymerase	Primer	Denature	Anneal	Extend
Promega GoTaq Green	<i>prickle1a</i> genotype	2 min. at 95°C (initial) 30 sec. at 95°C (x35)	30 sec. at 55 °C (x35)	30 sec. at 72 °C (x35) 5 min. at 72 °C (final)
Expand Long	<i>prickle1a</i> cDNA	2 min. at 94°C (initial) 15 sec. at 94°C (x35)	30 sec. at 59 °C (x35)	1 min. at 68 °C (x35) 5 min. at 68 °C (final)
Expand Long	<i>zfprickle1a</i> BamHI <i>zfprickle1a</i> XbaI	2 min. at 94°C (initial) 15 sec. at 94°C (x35)	30 sec. at 55 °C (x35)	2.5 min. at 68 °C (x35) 5 min. at 68 °C (final)
Promega GoTaq Green	<i>ctslb</i>	2 min. at 95°C (initial) 30 sec. at 95°C (x30)	30 sec. at 56 °C (x30)	30 sec. at 72 °C (x30) 5 min. at 72 °C (final)

Table 2. PCR parameters

RESULTS

Characterization of the *prickle1a* (sa24579) genetic mutation

Given that the sa24579 allele is a nonsense mutation in the *prickle1a* coding sequence, we initially hypothesized this lesion would represent a loss of function allele. To better understand the *prickle1a* (sa24579) genetic mutation, we first tested whether *prickle1a* transcripts were subjected to complete or partial nonsense mediated mRNA decay. Total RNA samples were obtained from tailbud stage wild type and mutant embryos. The tailbud stage is known to have high levels of *prickle1a* expression (White et al., 2017). Generated cDNA was PCR amplified using primers targeting a segment of the *prickle1a* coding sequence. Primer sequences chosen are separated by multiple introns and therefore allowed assessment of possible genomic DNA contamination (Figure 3.C). These primers span 27,470 bp of the *prickle1a* genomic locus, making them outside the amplification range of the chosen PCR conditions. In contrast, these primers span 1,109 bp on *prickle1a* cDNA, matching the size of the PCR amplified DNA fragments in Figure 5.A. The data show that there was a partial reduction of *prickle1a* mRNA levels in the mutant compared to wild type. The low yield of wild-type sample 2 (W2) is attributed to a lower yield of total RNA (Figure 5.A & B).

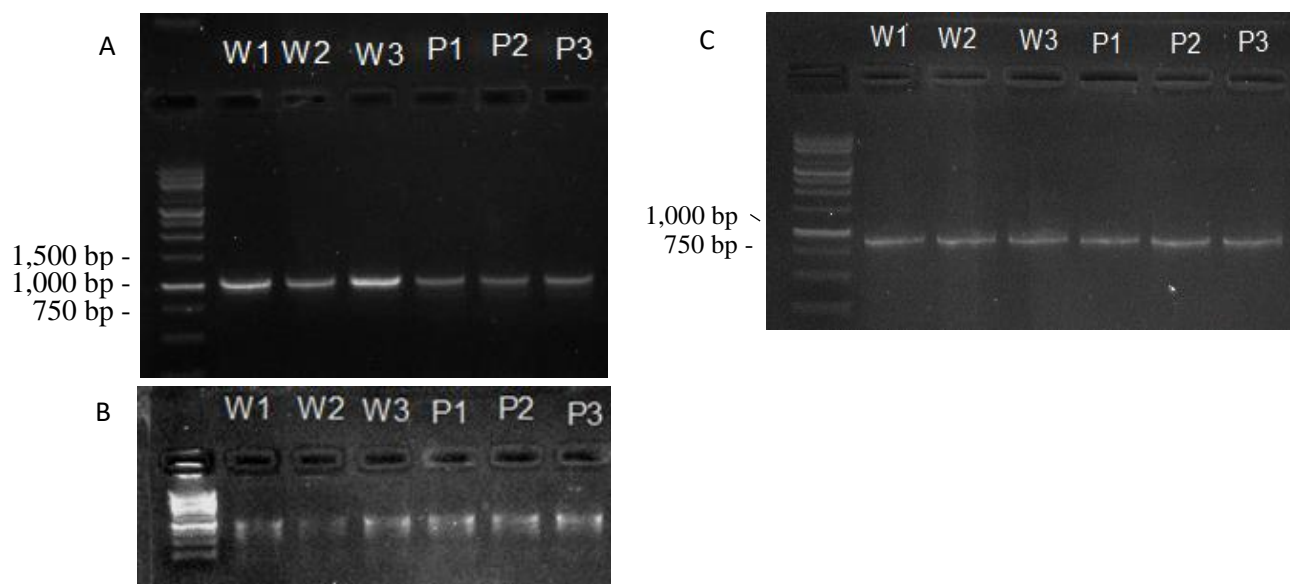


Figure 5. *prickle1a* sa24579 RT-PCR shows partial decay of *prickle1a* mRNA. (A) Wild type and *prickle1a* mutant complementary DNA (cDNA) was amplified via PCR with *prickle1a* cDNA primers. *prickle1a* samples (P1-P3) show decreased intensity compared to wild type (W1 and W3) (B) Total RNA samples were mixed with RNA loading buffer and run on a gel to determine quality of RNA. Lower intensity of wild type 3 (W3) compared to W1 and W2 correlates to Panel A (C) Wild type and *prickle1a* mutant cDNA was amplified via PCR with *ctslb* primers to demonstrate successful generation of cDNA. All samples were run on a 1% (w/v) agarose gel in TAE buffer and Biotium GelRed DNA stain alongside 10 μ L of Biotium 1kb Ready-to-Use DNA ladder.

The presence of *prickle1a* mRNA suggests that nonsense mediated mRNA decay occurred inefficiently and that translation of a truncated (596 amino acid; Figure 3.B) Prickle1a protein is possible. Injection of synthetic *prickle1a* mRNA into mutant embryos was performed to show suppression of the mutant phenotype. It is known that ectopic expression of genes encoding PCP proteins induces a C&E phenotype in gastrulation stage embryos (Jessen et al., 2002). Therefore, we first proved our *prickle1a* mRNA was functional by showing that overexpression in wild-type embryos induced a C&E phenotype at the tailbud stage, as indicated by a shortening of the anterior/posterior body axis (Figure 6.A & B). However, our attempts to suppress the mutant phenotype using various amounts of *prickle1a* mRNA showed no consistent difference between the non-injected control embryos and injected *prickle1a* homozygous mutants (Figure 6.C & D). One possible reason for this could be an inability to achieve the correct mRNA dose. We favor an alternative hypothesis where the *prickle1a* (sa24579) allele

represents a gain of function mutation, likely an antimorph or neomorph. Therefore, increased expression of Prickle1a protein (through *prickle1a* mRNA injection) would be unable to suppress the phenotype.

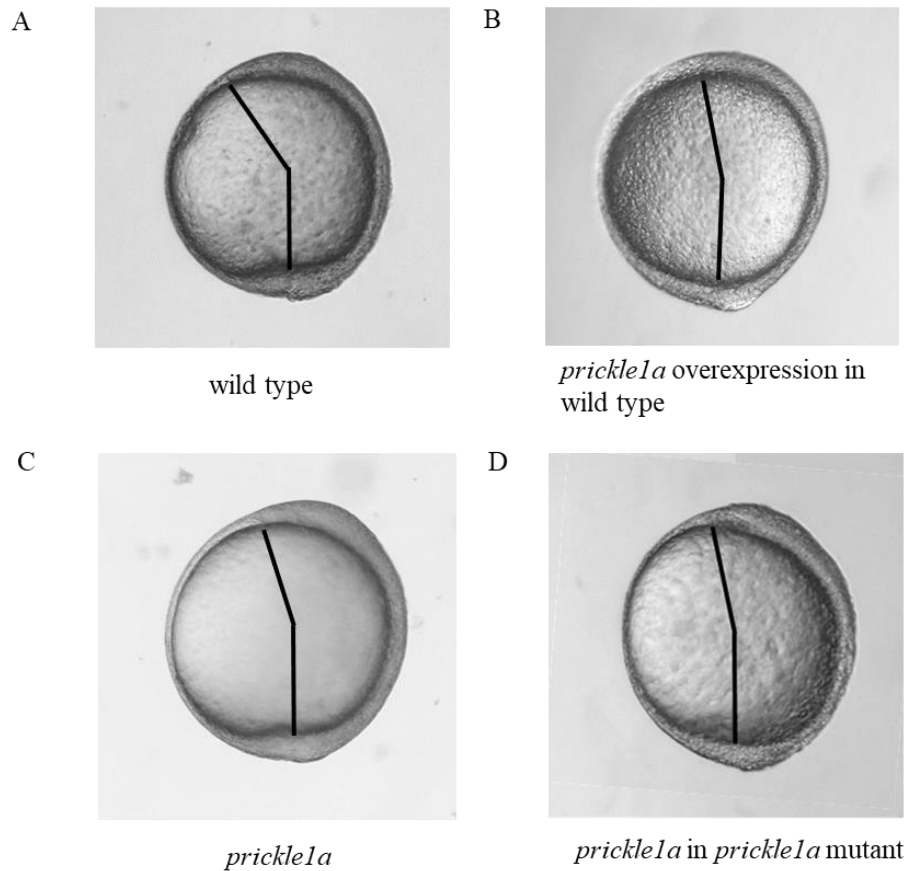


Figure 6. *prickle1a* fails to suppress a C&E phenotype in mutant embryos. Single cell stage mutant and wild-type embryos were injected with ~770 pg/embryo of *prickle1a* mRNA and imaged. (A) Lateral view of non-injected wild-type control at tailbud (B) Lateral view of *prickle1a* overexpression in wild type at tailbud. (C) Lateral view of non-injected *prickle1a* mutant control at tailbud. (D) Lateral view of injected *prickle1a* mutant at tailbud showing no suppression of the C&E phenotype. Black solid lines depict the posterior tailbud angle.

***prickle1a* (sa24579) mutant embryos display a C&E phenotype**

C&E defects are a hallmark of embryos with disrupted function of PCP proteins such as Vangl2 (Jessen et al., 2002). Therefore, we began our analyses of *prickle1a* homozygous mutant embryos by examining the narrowing and elongation of mutant body axes compared to wild type. These experiments used brightfield microscopy to image 1) live embryos and 2) fixed embryos subjected to whole mount in situ hybridization with a variety of probes that mark different embryonic tissues. While examining live embryos, it was noted that there was variability in the severity of the *prickle1a* mutant phenotype, and embryos were thus divided into three expressivity categories: mild, medium, and severe (Figure 7.C, E, & F). Of 93 embryos sampled, 28% showed mild expressivity, 37% showed medium expressivity, and 35% showed severe expressivity (Figure 7.G). Regardless, lateral images of live *prickle1a* mutant embryos from all three categories show a reduction in the length of the body axis compared to wild type (Figure 7.A, C, E, & F). Furthermore, there is distinct broadening of dorsal tissues in *prickle1a* mutant embryos that is observable in both live (Figure 7.B & D) and fixed embryos (Figure 8.B, C, E, & F). The neuroectodermal width of fixed embryos was measured using *distal-less homeobox 3b* (*dlx3*) antisense RNA WISH probe, resulting in a mean width of 1.38 in wild type and 1.72 in the mutant (Figure 8.G). The notochord (mesoderm) width of fixed embryos was measured using *T-box transcription factor Ta* (*tbxta*) antisense RNA WISH probe, resulting in a mean width of 0.10 in wild type and 0.16 in the mutant (Figure 8.H).

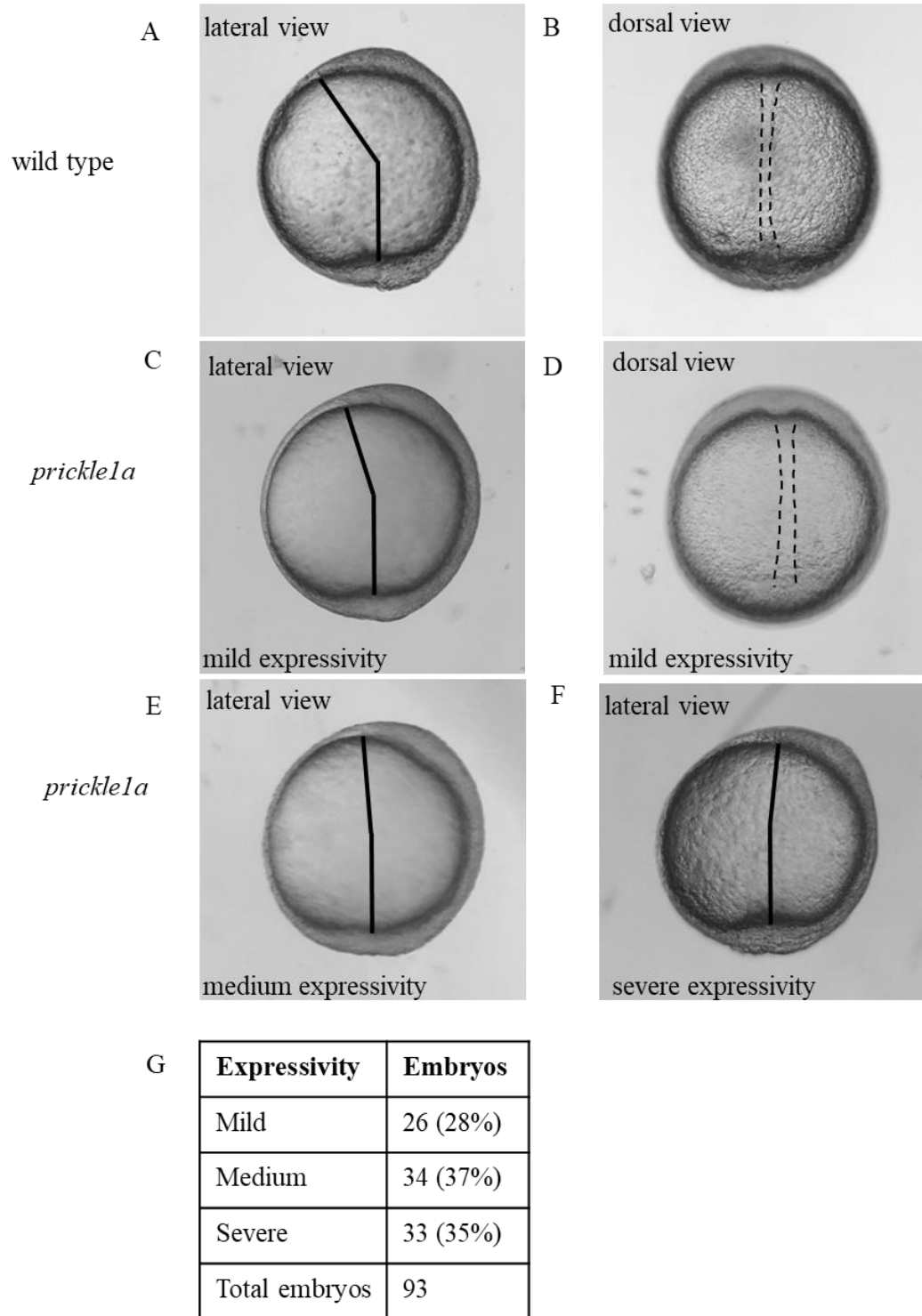


Figure 7. *prickle1a sa24579* results in a variable C&E phenotype represented by shortened anterior/posterior body axis and broader notochord at tailbud. (A) Lateral view of wild type at tailbud (B) Dorsal view of wild type at tailbud (C, E, & F) Lateral views of *prickle1a* mutant at tailbud showing variable expressivity (D) Dorsal view of *prickle1a* mutant at tailbud showing mild expressivity. (G) Amount and percentage of *prickle1a* mutant embryos showing each category of expressivity at tailbud. Black solid lines depict the posterior tailbud angle. Black dotted lines depict the notochord.

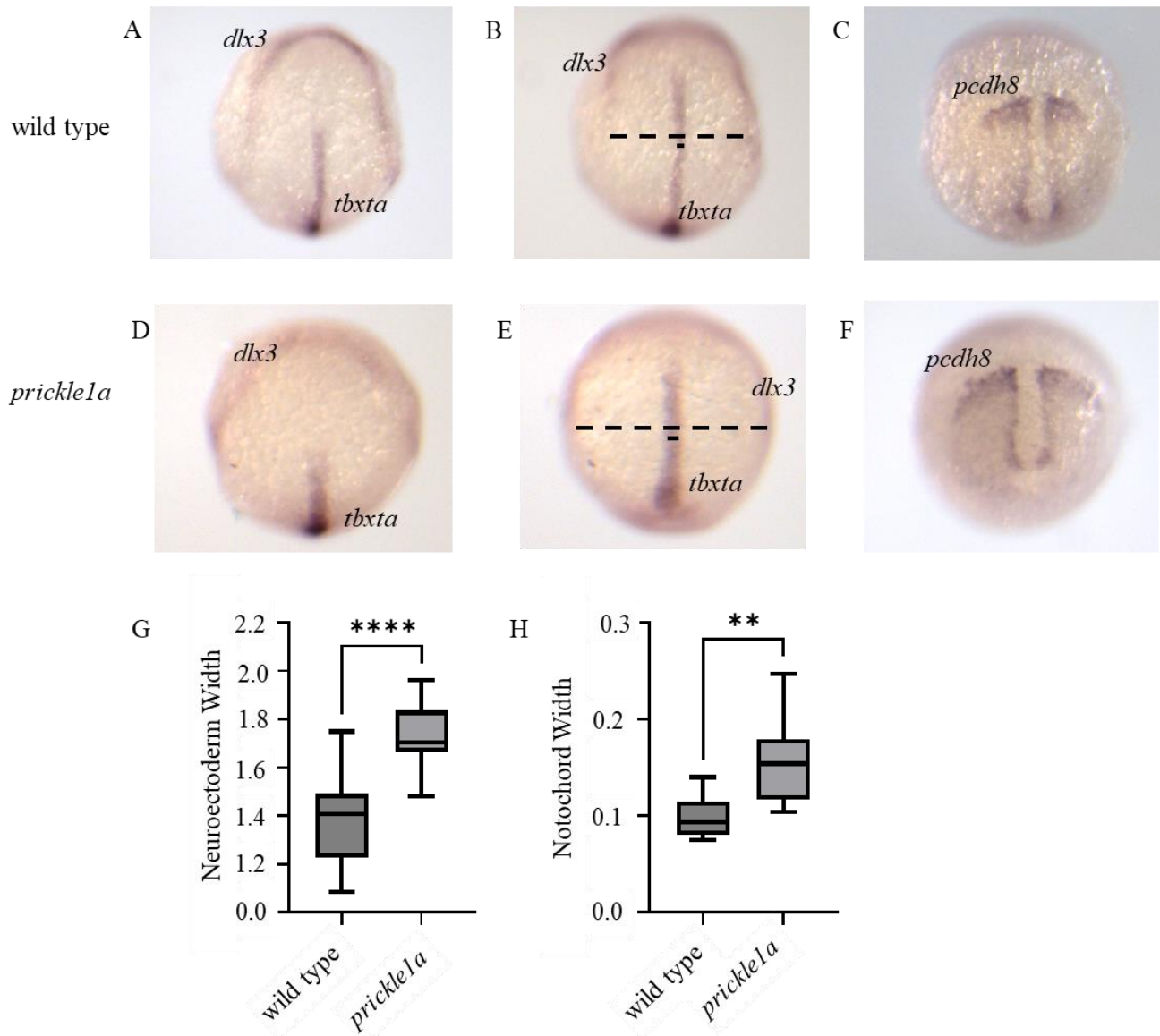


Figure 8. *prickle1a sa24579* whole mount *in situ* hybridization assays show further evidence of a C&E phenotype. Tailbud stage embryos labeled with neuroectoderm marker distal-less homeobox 3b (*dlx3*), notochord marker T-box transcription factor Ta (*tbxta*), and paraxial mesoderm marker protocadherin 8 (*pcdh8*). (A & D) Anterior view of the neuroectoderm and notochord in wild-type and mutant embryos. (B & E) Dorsal view of the neuroectoderm and notochord in wild-type and mutant embryos. (C & F) Dorsal view of the paraxial mesoderm in wild-type and mutant embryos. (G) Quantification of dorsal neuroectoderm width in wild-type versus *prickle1a* mutant embryos. Black solid lines in B and E represent approximate region measured. $n = 19$ (wild type), $n = 21$ (*prickle1a* mutant). (H) Quantification of notochord width in wild-type versus *prickle1a* mutant embryos. Black solid lines in B and E represent approximate region measured. $n = 7$ (wild type), $n = 9$ (*prickle1a* mutant). **** $P < 0.0001$, ** $P < 0.01$, unpaired Student's *t*-test with Welch's correction.

To further assess the *prickle1a* C&E mutant phenotype, one-cell stage wild type and mutant embryos were injected with a low (suboptimal) dose (~ 2.5 ng/embryo) of *vangl2* antisense MO oligonucleotide (Love et al., 2018). In wild type, this dose of MO induces a mild C&E phenotype (Figure 9) (Dohn et al., 2013). Injections of 2.5 ng *vangl2* MO into *prickle1a* mutant embryos

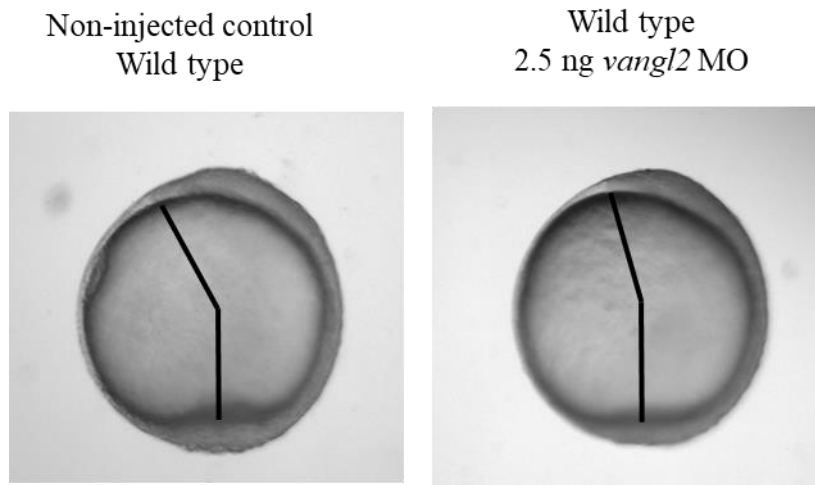
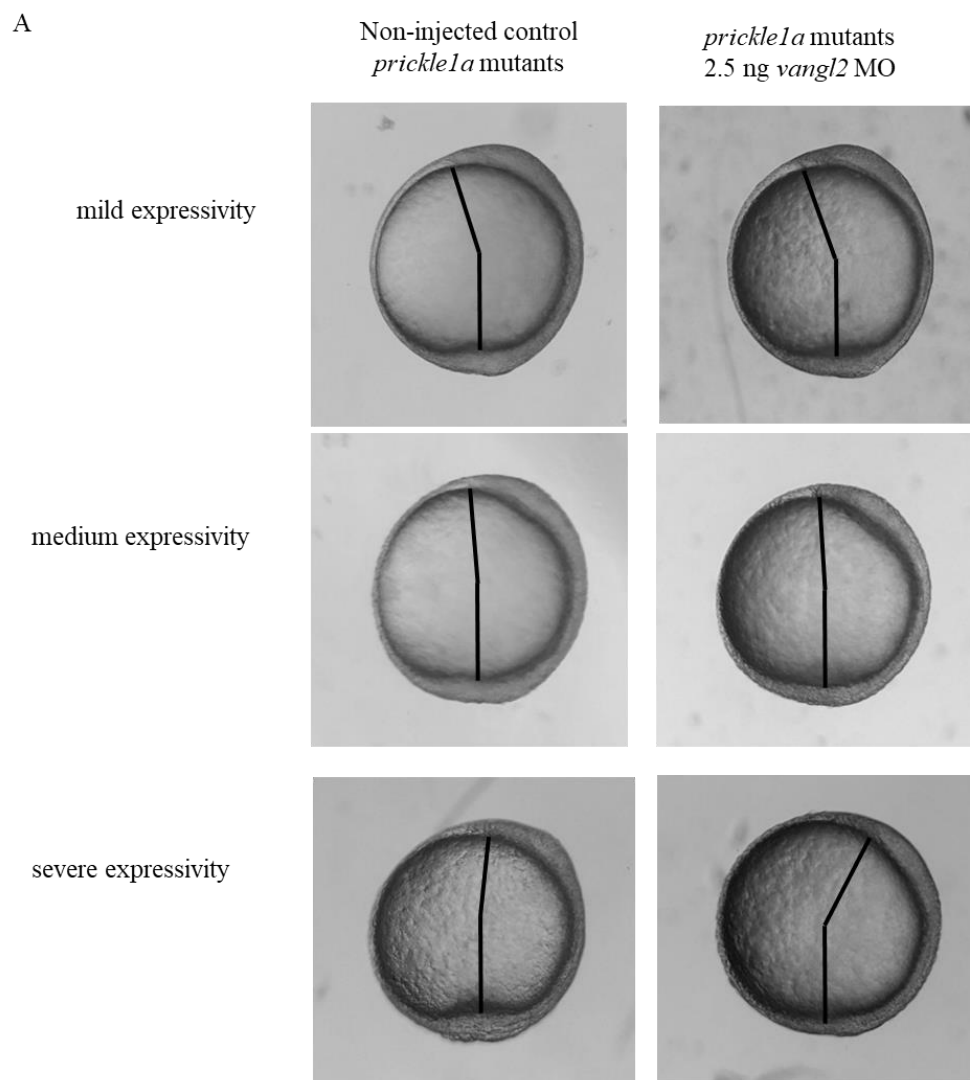


Figure 9. Low dose injection of *vangl2* antisense morpholino (MO) oligonucleotide into wild type. Single-cell stage wild-type embryos were injected with 2.5 ng/embryo of *vangl2* MO and examined at tailbud.

causes a worsening of the C&E phenotype seen at the tailbud stage compared to the varying levels of expressivity in non-injected mutants (Figure 10.A). Further analysis of injected embryos at 28 hours post fertilization also showed an enhancement of the *prickle1a* mutant phenotype (Figure 11). Of 20 injected embryos sampled, all showed varying degrees of an enhanced phenotype compared to control embryos (Figure 11.B). Together, these data support the notion that there is a genetic interaction between *prickle1a* and *vangl2*.

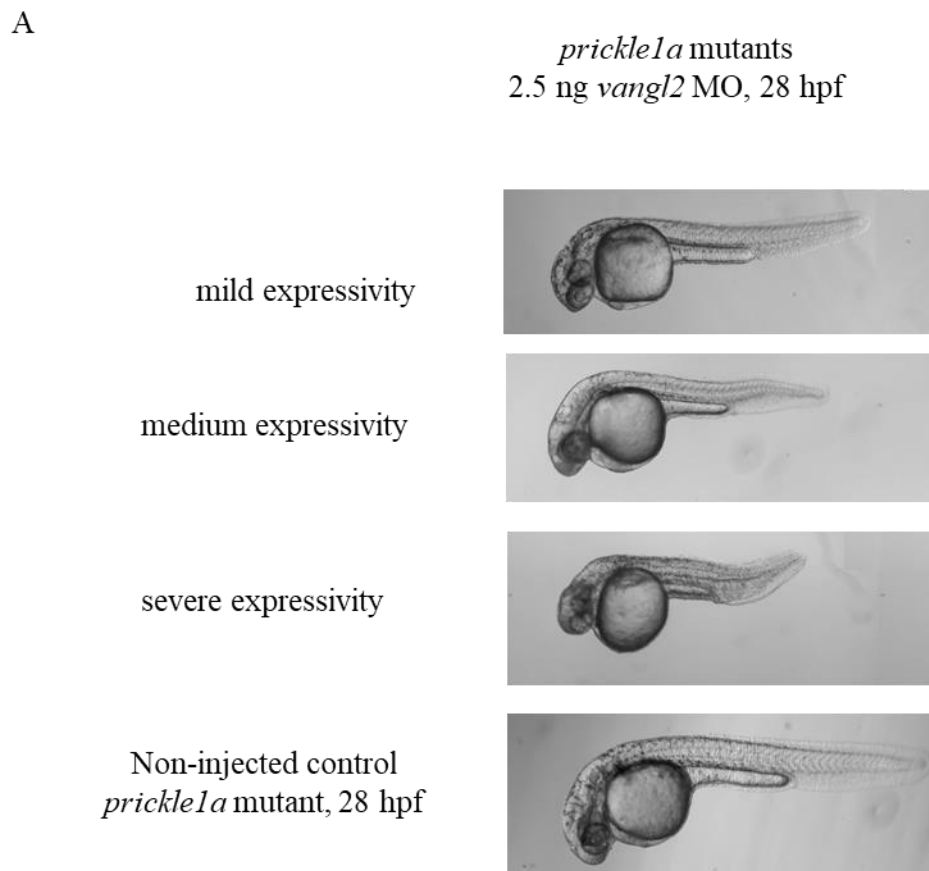
At the beginning of this project, it was assumed that like *vangl2/trilobite* mutant embryos (Solnica-Krezel et al., 1996), homozygous *prickle1a* sa24579 mutant embryos would not survive to adulthood. However, our data show that adult homozygous adults are viable and fertile. These findings indicate that the sa24579 mutation is not embryonic lethal.



B

Tailbud Non-injected Expressivity	Embryos	Tailbud Injection Expressivity	Embryos
Mild	8 (27%)	Mild	4 (13%)
Medium	14 (47%)	Medium	14 (47%)
Severe	8 (27%)	Severe	12 (40%)
Total embryos	30	Total embryos	30

Figure 10. Analysis of *vangl2* antisense morpholino (MO) oligonucleotide injected *prickle1a* mutant embryos. (A) Single-cell stage *prickle1a* mutant embryos were injected with 2.5 ng/embryo of *vangl2* MO and examined at the tailbud stage. Injected embryos were categorized based on severity and compared to non-injected control mutants. (B) Percentages of injected and non-injected embryos in each category.



B

28 hpf tailbud injection expressivity	Embryos
Mild	9 (45%)
Medium	7 (35%)
Severe	4 (20%)
Total embryos	20

Figure 11. Analysis of *vangl2* antisense morpholino (MO) oligonucleotide injected *prickle1a* mutant embryos at 28-hour post fertilization (hpf). (A) *vangl2* MO injected mutant embryos (2.5 ng/embryo). Non-injected mutant embryos show no apparent phenotype at 28 hpf. Injected mutant embryos show varying degrees of a mutant phenotype. (B) Percentages of injected mutant embryos in each category.

***prickle1a* (sa24579) mutant embryos display a PCP phenotype**

A fundamental requirement of C&E in ectodermal and mesodermal tissues is PCP. Extensive published data show that establishment of PCP in zebrafish gastrula cells is characterized by changes in cell elongation, alignment in relation to the body axes, and migration directness. Therefore, we next analyzed cell migratory behaviors and morphology in *prickle1a* mutant tailbud stage embryos. We focused our experiments on mesodermal cells as the majority of Vangl2 data was obtained from this germ layer (Jessen et al., 2002, Prince and Jessen, 2019). Figure 12 shows a disruption in cell migration directness in *prickle1a* mutant embryos. The cell migration tracks towards the dorsal axis show increased meandering in mutant embryos compared to wild type (Figure 12.A), and the average directness value of 0.46 in the mutant is significantly lower than 0.89 directness value obtained from wild-type cells (Figure 12.B). Furthermore, cell morphology analysis shows rounder, less packed cells in the *prickle1a* mutant compared to wild type (Figure 13). Wild-type length to width ratios averaged 1.65 versus 1.46 in

prickle1a mutant cells (Figure 10.D & E). Interestingly, there was not a significant difference in mediolateral cell alignment between wild type and *prickle1a* mutant embryos (Figure 13.C & E).

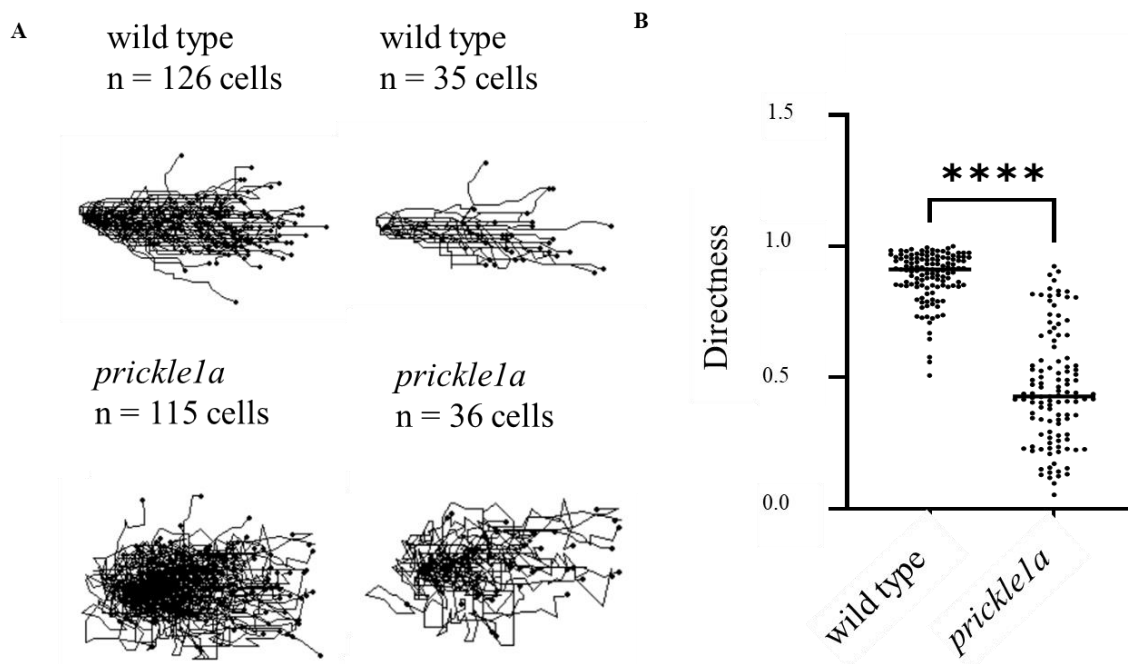


Figure 12. *prickle1a sa24579* mutation results in disruption of cell migration directness at the tailbud stage. (A) Cell migration tracks of wild type and *prickle1a* mutant embryos toward the dorsal axis. Reduced sample size tracks are shown for clarity. (B) Directness values for individual cells (wild type: n = 126 cells, 5 embryos; *prickle1a* mutant: n = 115 cells, 6 embryos). Scatter plot (B) shows individual data points and average values. **** $P < 0.0001$, unpaired Student's *t*-test with Welch's correction.

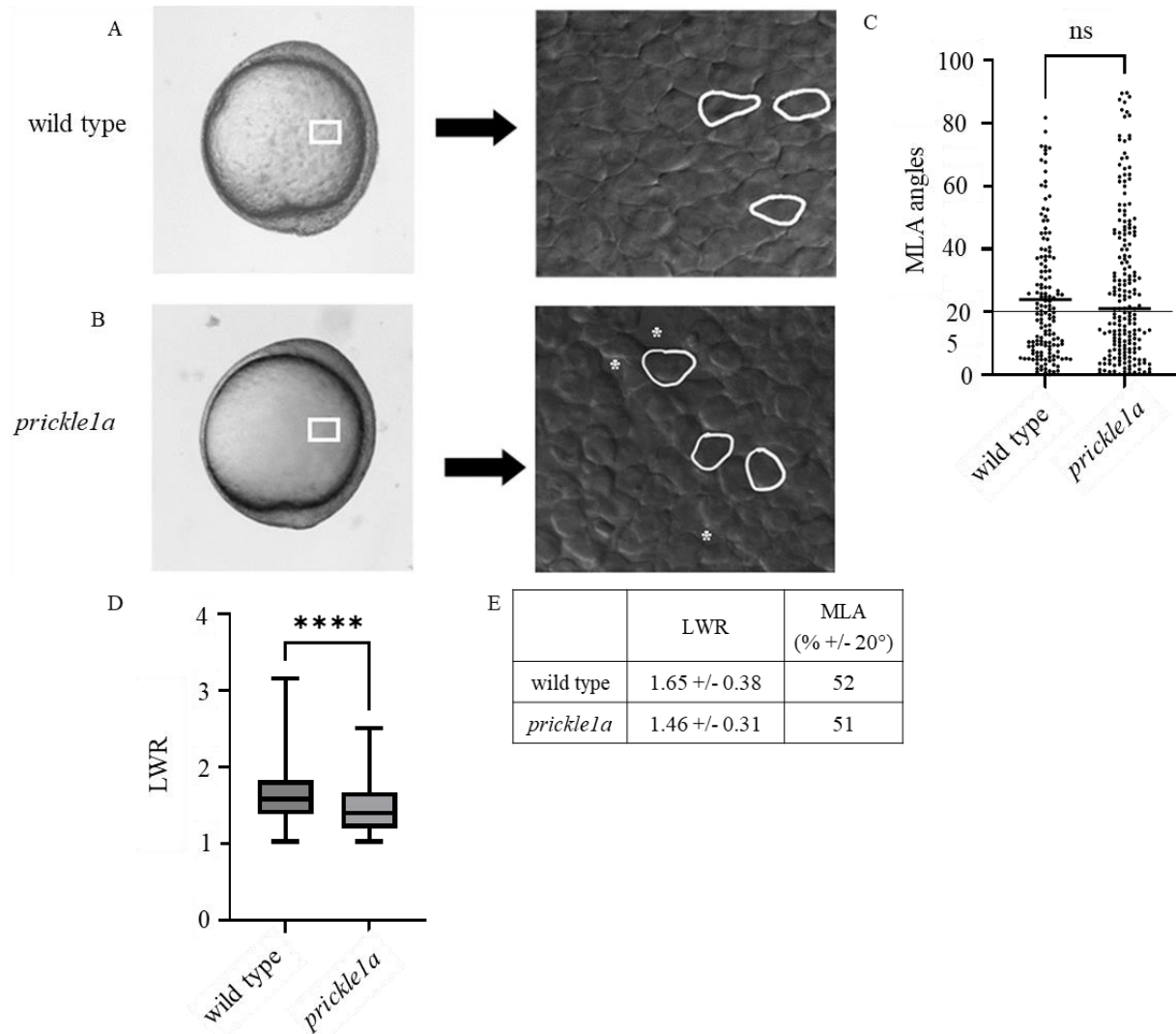


Figure 13. *prickle1a sa24579* mutation results in disruption of cell morphology but not orientation. (A & B) Live embryo (left) and DIC (right) images of wild type and *prickle1a* tailbud stage embryos. DIC images were taken at the mesodermal tissue layer and oriented as shown on the left with dorsal to the right and anterior to the top. Select cells are outlined to show elongation and alignment relative to the dorsal-ventral body axis. White asterisks represent spaces between cells. White boxes indicate approximate position of analysis. (C) Scatter plot showing medial lateral alignment (MLA) of individual mesodermal cells relative to the dorsal axis. Long black line indicates 20°. (D) Box plot showing length to width ratios (LWR) between wild type and *prickle1a* mutant mesodermal cells. (E) LWR and MLA averages from C and D (wild type: $n = 149$ cells, 8 embryos; *prickle1a* mutant: $n = 197$ cells, 11 embryos). **** $P < 0.0001$, ns = not significant, unpaired Student's *t*-test with Welch's correction.

DISCUSSION

Though the zebrafish genome encodes homologs of *Drosophila* core PCP proteins, it is unclear whether these proteins serve the same role in vertebrate PCP (Creighton & Jessen, 2021). It has been determined that Vangl2, an ortholog to *Drosophila* Vang/Stbm, is necessary for polarization of zebrafish gastrula cells. More specifically, Vangl2 is crucial for mediolateral cell polarity and membrane protrusion polarity that underlie proper C&E movements (Jessen et al., 2002; Love et al., 2018; Prince & Jessen, 2019). However, there still exists many gaps regarding the function of zebrafish and other vertebrate PCP proteins. One of five zebrafish Prickle homologs, Prickle1a was identified as the most like *Drosophila* Pk and is expressed in lateral ectodermal and mesendodermal tissues during gastrulation (Veeman, et al., 2003). Due to inconsistencies in reported C&E data regarding Prickle1a (Carreira-Barbosa et al. 2003; Veeman et al. 2003; Ahsan et al. 2019), it was important to clearly determine and document the presence of a C&E phenotype and thoroughly evaluate the requirement for Prickle1a function during PCP in the zebrafish gastrula embryo.

To better understand Prickle1a, we needed to determine how the *prickle1a* (sa24579) zebrafish mutant model works at the genetic level. Therefore, we performed RT-PCR on cDNA generated from *prickle1a* mutant embryos and observed a reduction, but not total absence, of mutant compared to wild type expression levels. The efficiency of nonsense mediated mRNA decay (NMD) is known to vary among cell types (Sato and Sanger, 2021; Linde et al., 2007), and this may explain why *prickle1a* transcripts remain present in homozygous mutant embryos. Another cause of NMD deficiency could be stop codon positioning (Khajavi et al. 2006). The *prickle1a* (sa24579) nonsense mutation lies in the final exon of the transcript (Figure 3). In mammals, most studies suggest that at least one intron must occur after the stop codon to allow

differentiation between a premature stop codon and the normal stop codon (Nagy & Maquat, 1998). If the NMD pathway is unable to recognize a premature stop codon in the final exon, it is possible for a transcript to escape decay and be translated into a protein (Khajavi et al. 2006). However, some studies have shown that, while not as effective, premature stop codons can result in NMD-mediated mRNA reduction even in the absence of a downstream intron (Bühler et al., 2006).

Because a truncated version of Prickle1a may be translated in the homozygous mutant embryos, it is possible that this abnormal protein interferes with PCP through an antimorphic or neomorphic activity. This notion is supported by our inability to suppress the mutant C&E phenotype through injection of synthetic *prickle1a* mRNA, as it suggests that the sa24579 is not a loss of function allele. Earlier studies have shown that the C-terminus of Prickle1a contains a prenylation sequence that may be responsible for its localization (Veeman et al., 2003). As mentioned, Prickle1a also physically binds and at least partially regulates Vangl2 enrichment at the plasma membrane (Dohn et al., 2013). Therefore, a version of Prickle1a missing this prenylation sequence may inhibit proper localization and therefore function of Vangl2 at the cell surface. If a truncated Prickle1a is translated and stable in homozygous mutants, co-immunoprecipitation assays and cell localization studies could show whether Vangl2 function is disrupted in homozygous *prickle1a* mutants. Further cell imaging experiments would also be necessary to show where this version of Prickle1a localizes in gastrula cells compared to wild-type protein. These studies may support the notion that lack of the C-terminal prenylation sequence contributes to the *prickle1a* mutant PCP phenotype.

It is also possible that a truncated Prickle1a protein is unstable and degraded. C-terminal protein truncations have been shown to result in reduced protein stability (Koch et al., 2014), and

subsequently lead to proteasomal degradation (Jackson & Hewitt, 2016). Western blots using an antibody targeting an epitope found in both wild type and mutant Prickle1a will be necessary to further evaluate the presence and level of truncated Prickle1a protein in mutant embryos. In addition, injection of synthetic mRNA encoding the Prickle1a sa24579 mutant protein into wild-type embryos can be used to assess translation and induction of both C&E and PCP phenotypes.

Regardless of the genetic nature of the *prickle1a* sa24579 allele, both C&E and PCP phenotypes are present. Two important PCP-dependent morphological events occur during zebrafish gastrulation: mediolateral intercalation of midline cells and dorsal migration of lateral cells (Creighton & Jessen, 2021). One consequence of midline cells failing to undergo effective mediolateral intercalation is broadening of the notochord and shortening of the anterior/posterior axis as observed with disrupted C&E (Warga & Kimmel, 1990). The broadened notochord and shortened body axis, along with the less directed dorsal cell migration seen in the *prickle1a* (sa24579) mutants indicate a disruption in PCP polarization of gastrula cells. However, another indicator of abnormal PCP is a lack of mediolateral cellular alignment perpendicular to the dorsal embryonic body axis (Jessen et al., 2002). Interestingly, there is no significant difference in the alignment of mutant lateral cells compared to wild type, indicating that there is no interference with this process in the mutant. One characteristic of PCP is the ability of cells to communicate between each other to coordinate their polarization (Goodrich & Strutt, 2011). In the context of zebrafish PCP, this coordinated polarization would include the mediolateral alignment of gastrula cells. It is possible that lack of disrupted mediolateral alignment in the mutant means Prickle1a is not essential for the intercellular communication that drives this process. Previous fly studies support this idea, as null *prickle* mutant clones introduced to wild-type tissue had no significant impact on trichome orientation in non-mutant tissue, indicating Prickle is not essential

for intercellular communication in the fly (Strutt & Strutt, 2007). Like data on zebrafish Vangl2 (Jessen et al., 2002), ectopic expression of synthetic *prickle1a* mRNA in wild-type embryos induced a C&E phenotype as indicated by shortening of the anterior/posterior body axis (Figure 6). Additionally, knockdown of Vangl2 expression in *prickle1a* mutant embryos enhanced the C&E phenotype, demonstrating a genetic interaction between *vangl2* and *prickle1a*.

While the underlying molecular defect of the *prickle1a* (sa24579) mutation has not been fully elucidated, this study clearly demonstrates that Prickle1a is required for proper PCP establishment during zebrafish gastrulation. Mutation of the *prickle1a* gene results in disruption of effective C&E movements, likely due to decreased mediolateral intercalation of midline cells and disruption of dorsal convergence of lateral cells. Whether this phenotype is due to reduced *prickle1a* expression or expression of an abnormal truncated Prickle1a protein will be the focus of future research.

REFERENCES

- Ahsan, K., Singh, N., Rocha, M., Huang, C., Prince, V.E. (2019) Prickle1 is required for EMT and migration of zebrafish cranial neural crest. *Developmental Biology*. 448(1):16-35.
- Bastock, R., Strutt, H., & Strutt, D. (2003). Strabismus is asymmetrically localised and binds to Prickle and Dishevelled during *Drosophila planar* polarity patterning. *Development (Cambridge, England)*, 130(13), 3007–3014. <https://doi.org/10.1242/dev.00526>
- Bühler, M., Steiner, S., Mohn, F., Paillusson, A., & Mühlemann, O. (2006). EJC-independent degradation of nonsense immunoglobulin- μ mRNA depends on 3' UTR length. *Nature structural & molecular biology*, 13(5), 462–464. <https://doi.org/10.1038/nsmb1081>
- Busch-Nentwich, E., Kettleborough, R., Dooley, C. M., Scahill, C., Sealy, I., White, R., Herd, C., Mehroke, S., Wali, N., Carruthers, S., Hall, A., Collins, J., Gibbons, R., Pusztai, Z., Clark, R., and Stemple, D.L. (2013) Sanger Institute Zebrafish Mutation Project mutant data submission. ZFIN Direct Data Submission. (<http://zfin.org>).
- Carreira-Barbosa, F., Concha, M. L., Takeuchi, M., Ueno, N., Wilson, S. W., & Tada, M. (2003). Prickle 1 regulates cell movements during gastrulation and neuronal migration in zebrafish. *Development (Cambridge, England)*, 130(17), 4037–4046. <https://doi.org/10.1242/dev.00567>
- Caswell, P. T., & Zech, T. (2018). Actin-Based Cell Protrusion in a 3D Matrix. *Trends in cell biology*, 28(10), 823–834. <https://doi.org/10.1016/j.tcb.2018.06.003>
- Creighton, J.H., Jessen, J.R. (2021). Core pathway proteins and the molecular basis of planar polarity in the zebrafish gastrula. *Seminars in Cell and Developmental Biology*, <https://doi.org/10.1016/j.semcdb.2021.09.015>

Dohn, M. R., Mundell, N. A., Sawyer, L. M., Dunlap, J. A., & Jessen, J. R. (2013). Planar cell polarity proteins differentially regulate extracellular matrix organization and assembly during zebrafish gastrulation. *Developmental biology*, 383(1), 39–51.

<https://doi.org/10.1016/j.ydbio.2013.08.027>

Gilmour, D. T., Jessen, J. R., Lin, S., Nusslein-Volhard, C. (Ed.), & Dahm, R. (Ed.) (2002). Manipulating gene expression in the zebrafish. In *Zebrafish, a Practical Approach* (Vol. 261, pp. 121–143). essay, Oxford University Press.

Goodrich, L. V., Strutt, D. (2011). Principles of planar polarity in animal development.

Development 138(10). doi:10.1242/dev.054080

Hale, R., & Strutt, D. (2015). Conservation of Planar Polarity Pathway Function Across the Animal Kingdom. *Annual review of genetics*, 49, 529–551.

<https://doi.org/10.1146/annurev-genet-112414-055224>

Harrison, C., Shao, H., Strutt, H., & Strutt, D. (2020). Molecular mechanisms mediating asymmetric subcellular localisation of the core planar polarity pathway proteins. *Biochemical Society transactions*, 48(4), 1297–1308.

<https://doi.org/10.1042/BST20190404>

Jackson, M. P., & Hewitt, E. W. (2016). Cellular proteostasis: degradation of misfolded proteins by lysosomes. *Essays in biochemistry*, 60(2), 173–180.

<https://doi.org/10.1042/EBC20160005>

Jessen, J. R., Topczewski, J., Bingham, S., Sepich, D. S., Marlow, F., Chandrasekhar, A. and Solnica-Krezel, L. (2002). Zebrafish trilobite identifies new roles for Strabismus in gastrulation and neuronal movements. *Nat. Cell Biol.* 4, 610-615. doi:10.1038/ncb828

- Jessen, J. R., Solnica-Krezel, L. (2005). Morphogenetic cell movements shaping the zebrafish gastrula. *Advances in Developmental Biology* 14. 131-165.
[https://doi.org/10.1016/S1574-3349\(05\)14007-1](https://doi.org/10.1016/S1574-3349(05)14007-1)
- Jessen, J. R. (2012). Analyzing planar cell polarity during zebrafish gastrulation. *Methods in molecular biology (Clifton, N.J.)*, 839, 69–78. https://doi.org/10.1007/978-1-61779-510-7_6
- Kettleborough, R. N., Busch-Nentwich, E. M., Harvey, S. A., Dooley, C. M., de Bruijn, E., van Eeden, F., Sealy, I., White, R. J., Herd, C., Nijman, I. J., Fényes, F., Mehroke, S., Scahill, C., Gibbons, R., Wali, N., Carruthers, S., Hall, A., Yen, J., Cuppen, E., & Stemple, D. L. (2013). A systematic genome-wide analysis of zebrafish protein-coding gene function. *Nature*, 496(7446), 494–497. <https://doi.org/10.1038/nature11992>
- Kimmel, C. B., Ballard, W. W., Kimmel, S. R., Ullmann, B., & Schilling, T. F. (1995). Stages of embryonic development of the zebrafish. *Developmental dynamics : an official publication of the American Association of Anatomists*, 203(3), 253–310.
<https://doi.org/10.1002/aja.1002030302>
- Koch, B., Schmidt, C., Ploier, B., & Daum, G. (2014). Modifications of the C terminus affect functionality and stability of yeast triacylglycerol lipase Tgl3p. *The Journal of biological chemistry*, 289(28), 19306–19316. <https://doi.org/10.1074/jbc.M114.556944>
- Love, A. M., Prince, D. J., Jessen, J. R. (2018). Vangl2-dependent regulation of membrane protrusions and directed migration requires a fibronectin extracellular matrix. *Development*, 145(22). doi:10.1242/dev.165472
- Nagy E., Maquat L.E. (1998). A rule for termination-codon position within intron-containing genes: when nonsense affects RNA abundance. *Trends Biochem Sci* 1998; 23: 198– 199.

- Nüsslein-Volhard, C. (2012). The zebrafish issue of *Development*. *Development (Cambridge, England)*, *139*(22), 4099–4103. <https://doi.org/10.1242/dev.085217>
- Prince, D. J., Jessen, J. R. (2019). Dorsal convergence of gastrula cells requires Vangl2 and an adhesion protein-dependent change in protrusive activity. *Development*, *146*(22). doi:10.1242/dev.182188
- Roszko, I., Sawada, A., & Solnica-Krezel, L. (2009). Regulation of convergence and extension movements during vertebrate gastrulation by the Wnt/PCP pathway. *Seminars in cell & developmental biology*, *20*(8), 986–997. <https://doi.org/10.1016/j.semcdb.2009.09.004>
- Sepich, D. S., Myers, D. C., Short, R., Topczewski, J., Marlow, F., & Solnica-Krezel, L. (2000). Role of the zebrafish trilobite locus in gastrulation movements of convergence and extension. *Genesis*, *27*(4), 159-173. [https://doi.org/10.1002/1526-968X\(200008\)27:4<159::AID-GENE50>3.0.CO;2-T](https://doi.org/10.1002/1526-968X(200008)27:4<159::AID-GENE50>3.0.CO;2-T)
- Sepich, D. S., Calmelet, C., Kiskowski, M., & Solnica-Krezel, L. (2005). Initiation of convergence and extension movements of lateral mesoderm during zebrafish gastrulation. *Developmental dynamics: an official publication of the American Association of Anatomists*, *234*(2), 279–292. <https://doi.org/10.1002/dvdy.20507>
- Solnica-Krezel, L., Schier, A. F., & Driever, W. (1994). Efficient recovery of ENU-induced mutations from the zebrafish germline. *Genetics*, *136*(4), 1401–1420. <https://doi.org/10.1093/genetics/136.4.1401>
- Solnica-Krezel, L., Stemple, D. L., Mountcastle-Shah, E., Rangini, Z., Neuhauss, S. C., Malicki, J., Schier, A. F., Stainier, D. Y., Zwartkuis, F., Abdelilah, S., & Driever, W. (1996). Mutations affecting cell fates and cellular rearrangements during gastrulation in

- zebrafish. *Development (Cambridge, England)*, 123, 67–80.
<https://doi.org/10.1242/dev.123.1.67>
- Strutt, H., & Strutt, D. (2005). Long-range coordination of planar polarity in *Drosophila*. *BioEssays: news and reviews in molecular, cellular and developmental biology*, 27(12), 1218–1227. <https://doi.org/10.1002/bies.20318>
- Strutt, D., & Strutt, H. (2007). Differential activities of the core planar polarity proteins during *Drosophila* wing patterning. *Developmental biology*, 302(1), 181–194.
<https://doi.org/10.1016/j.ydbio.2006.09.026>
- Taylor, J., Abramova, N., Charlton, J., & Adler, P. N. (1998). Van Gogh: a new *Drosophila* tissue polarity gene. *Genetics*, 150(1), 199–210.
<https://doi.org/10.1093/genetics/150.1.199>
- Tree, D. R., Shulman, J. M., Rousset, R., Scott, M. P., Gubb, D., & Axelrod, J. D. (2002). Prickle mediates feedback amplification to generate asymmetric planar cell polarity signaling. *Cell*, 109(3), 371–381. [https://doi.org/10.1016/s0092-8674\(02\)00715-8](https://doi.org/10.1016/s0092-8674(02)00715-8)
- Veeman, M. T., Slusarski, D. C., Kaykas, A., Louie, S. H., & Moon, R. T. (2003). Zebrafish prickle, a modulator of noncanonical Wnt/Fz signaling, regulates gastrulation movements. *Current biology: CB*, 13(8), 680–685. [https://doi.org/10.1016/s0960-9822\(03\)00240-9](https://doi.org/10.1016/s0960-9822(03)00240-9)
- Veldman, M., Lin, S. Zebrafish as a Developmental Model Organism for Pediatric Research. *Pediatr Res* 64, 470–476 (2008).
<https://doi.org/10.1203/PDR.0b013e318186e609>

- Vinson, C. R., & Adler, P. N. (1987). Directional non-cell autonomy and the transmission of polarity information by the frizzled gene of *Drosophila*. *Nature*, 329(6139), 549–551. <https://doi.org/10.1038/329549a0>
- Warga, R. M., & Kimmel, C. B. (1990). Cell movements during epiboly and gastrulation in zebrafish. *Development (Cambridge, England)*, 108(4), 569–580. <https://doi.org/10.1242/dev.108.4.569>
- Westerfield, M. (2000). *The Zebrafish Book. A Guide for the Laboratory Use of Zebrafish (Danio rerio)* (4th Ed.). University of Oregon Press.
- White RJ, Collins JE, Sealy IM, et al. (2017). A high-resolution mRNA expression time course of embryonic development in zebrafish. *Elife*. Nov;6:e30860. DOI: 10.7554/elifesciences.30860. PMID: 29144233; PMCID: PMC5690287.
- You, K. T., Li, L. S., Kim, N. G., Kang, H. J., Koh, K. H., Chwae, Y. J., Kim, K. M., Kim, Y. K., Park, S. M., Jang, S. K., & Kim, H. (2007). Selective translational repression of truncated proteins from frameshift mutation-derived mRNAs in tumors. *PLoS biology*, 5(5), e109. <https://doi.org/10.1371/journal.pbio.0050109>